High-resolution monochromator for iron nuclear resonance vibrational spectroscopy of biological samples

2016 Jpn. J. Appl. Phys. 55 122401

(http://iopscience.iop.org/1347-4065/55/12/122401)

Japanese Journal of Applied Physics **55**, 122401 (2016)
http://doi.org/10.7567/JJAP.55.122401

REGULAR PAPER

High-resolution monochromator for iron nuclear resonance vibrational spectroscopy of biological samples

Yoshitaka Yoda[1]*, Kyoko Okada[1], Hongxin Wang[2], Stephen P. Cramer[2], and Makoto Seto[3]

[1]*Japan Synchrotron Radiation Research Institute (JASRI), SPring-8, Sayo, Hyogo 679-5198, Japan*
[2]*Department of Chemistry, University of California, Davis, CA 95616, U.S.A.*
[3]*Research Reactor Institute, Kyoto University, Kumatori, Osaka 590-0494, Japan*

*E-mail: yoda@spring8.or.jp

Received May 12, 2016; revised September 13, 2016; accepted September 16, 2016; published online November 8, 2016

A new high-resolution monochromator for 14.4-keV X-rays has been designed and developed for the Fe nuclear resonance vibrational spectroscopy of biological samples. In addition to high resolution, higher flux and stability are especially important for measuring biological samples, because of the very weak signals produced due to the low concentrations of Fe-57. A 24% increase in flux while maintaining a high resolution better than 0.9 meV is achieved in the calculation by adopting an asymmetric reflection of Ge, which is used as the first crystal of the three-bounce high-resolution monochromator. A 20% increase of the exit beam size is acceptable to our biological applications. The higher throughput of the new design has been experimentally verified. A fine rotation mechanics that combines a weak-link hinge with a piezoelectric actuator was used for controlling the photon energy of the monochromatic beam. The resulting stability is sufficient to preserve the intrinsic resolution.

1. Introduction

Nuclear resonance vibrational spectroscopy (NRVS), also called nuclear inelastic scattering, is a unique spectroscopic method that can focus on the vibrations of a specific isotope.[1,2] The NRVS of Fe-57, with a resonant energy of 14.4 keV, is widely used among the available Mössbauer isotopes. NRVS is recognized as a powerful technique for probing the dynamics of the Fe active centers in many metalloproteins. Biological samples, such as enzymes and hemoproteins, have been intensively studied using NRVS.[3–7]

In NRVS experiments, a high-resolution monochromator (HRM) is placed after a high-heat-load monochromator and before the sample to produce X-rays with narrow energy bandwidth. Its high resolution is essential because it determines the resolution of the measured spectrum. The resolution of the HRM in the NRVS of biological samples is usually set to less than 1 meV in order to be able to distinguish the different vibrational modes. This resolution is also important for resolving the energy shifts resulting from isotope substitution between C-12 and C-13, N-14 and N-15, O-16 and O-18, S-32 and S-36, and so on.[8] These shifts yield very useful information for assigning the vibrational modes. However, the throughput of the HRM usually decreases as the resolution increases. A balanced trade-off between resolution and flux is required as both are important in NRVS experiments.

One of the serious problems for the NRVS of biological samples is that the delayed signal is quite weak, even if they are Fe-57 enriched. The Fe concentrations are low due to the macromolecules in solution. Furthermore, some vibrational peaks from light atoms such as Fe–C, Fe–N, and Fe–O appear at high frequencies with lower transition probabilities.[9] Small peaks can sometimes be buried statistically in background noise of ~5 counts per 100 s. Thus a higher incident flux from the HRM contributes not only to reducing the acquisition time, but also to the emergence of small interesting peaks, such as Fe–CO or even Ni–H–Fe inside a hydrogenase enzyme. Therefore, a higher flux from the HRM while maintaining the energy resolution benefits all NRVS experiments, and is a great help in the study of vibrational modes in biological samples.

Besides resolution and flux, the other feature required for HRM is its stability. This is particularly important for the NRVS of biological samples since scans are repeated multiple times to obtain sufficient statistics. For example, scans of one biological sample may be repeated 30 times taking 40 min/scan.

In NRVS spectra, the intensity of the delayed signal is recorded as a function of the crystal angle(s) in the HRM. The resonant peak position usually shifts or fluctuates with each scan due to temperature drift and/or mechanical drift of crystal angles. In the process of summing the scan data, the zero point of the phonon energy is easily calibrated from the resonant peak position for each NRVS scan. However, the drift during one scan is not taken into account, because of which the resolution of the summed spectra may become lower than the intrinsic resolution.

2. Monochromator design and mechanics

Several types of HRMs for Fe NRVS have been proposed and realized. These include a nested type,[10] a three-bounce type,[11] and a four-bounce type.[12,13] A resolution of less than 1 meV has been realized with the latter two types. We adopted the three-bounce type HRM, which consists of three reflecting crystals: (i) Ge 331, (ii) first Si 975, and (iii) second Si 975. The Ge reflection makes an output beam direction almost in a horizontal plane. The beam leaves the HRM with an upward angle of 0.3°. The two Si 975 crystals are arranged in (+, +), as shown in Fig. 1(a). A merit of this geometry is that the output X-ray energy is determined only by the angle between the two Si 975 crystals, provided the temperatures of the crystals are kept constant. All other factors have little or no effect on the output X-ray energy, so we focus only on the angle between the two Si 975 crystals when considering energy stability.

A conventional three-bounce monochromator consists of a symmetric Ge 331 reflection, a Si 975 reflection with an asymmetric factor of b, and a Si 975 reflection with an asymmetric factor of $1/b$. This yields an output beam whose size is the same as that of the incoming beam.

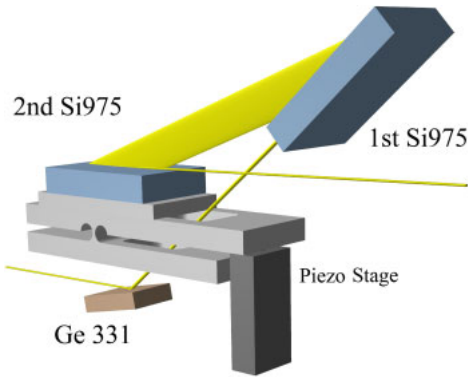

(a)

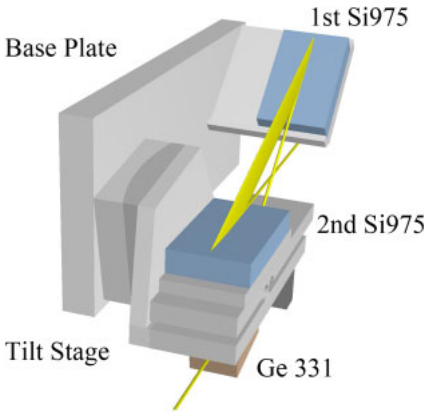

(b)

Fig. 1. (Color online) (a) HRM for the Fe NRVS and the X-ray beam trace, which involves three reflections: Ge 331, first Si 975, and second Si 975. (b) HRM with a base plate viewed from a different point. A height adjustment stage of the 1st Si 975 and a coarse rotating stage of the 2nd Si 975 are not shown for the sake of clarity. The angle between the two Si 975 crystals is controlled using the piezoelectric linear stage with a 25 μm stroke. Rotation is achieved using the tangent bar mechanism with setting the weak-link as the fulcrum line.

Table I. Crystal parameters for the newly designed HRM for the Fe NRVS of biological samples.

	Ge 331	1st Si 975	2nd Si 975
Bragg angle (°)	19.4	80.4	80.4
Asymmetric factor	1/2.0	1/10.8	18.0

A new HRM with higher throughput and the same resolution has been designed with the parameters listed in Table I. The unique idea for realizing higher throughput in the three-bounce-type device is to make the asymmetry of the 1st and 2nd Si 975 reflections as small as possible, while maintaining its resolution. This is because the reflectivity of an asymmetric reflection decreases as asymmetry increases due to absorption in the crystal. For example, the reflectivity of Si 975 for 14.4-keV X-rays with $b = 1/10.8$ is approximately 10% higher than that with $b = 1/18.0$. In practice, reflectivity with a larger asymmetry can be further reduced by the influence of surface conditions and surface lattice distortions. Smaller asymmetry was realized by adopting the asymmetric Ge reflection and a 20% larger output vertical beam size. At the Nuclear Resonant Scattering Beamline, BL09XU, SPring-8, the vertical size of the beam incident on

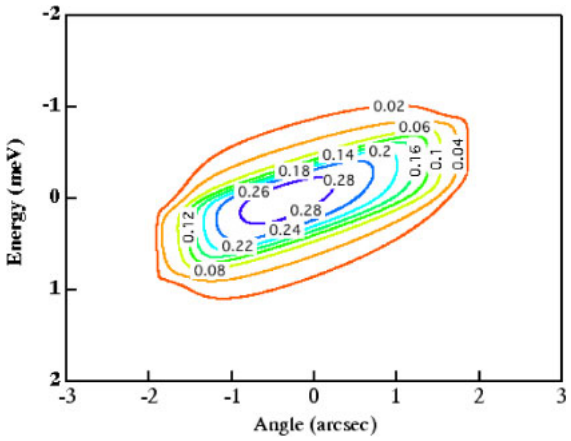

Fig. 2. (Color online) Calculated throughput (the Dumond diagram) of the newly designed HRM with double Si 111 reflections for 14.4-keV X-rays. The acceptance beam profile is shown. The maximum throughput is 0.299.

the HRM is 0.5 mm (full width at half maximum, FWHM). Thus, even if the beam size is enlarged in the vertical direction, the effect on measuring biological samples (usually ∼1 mm in the vertical direction) is not critical.

Figure 2 shows the contour plot of the throughput by calculation using the dynamical theory of X-ray diffraction, often called the Dumond diagram. An acceptance beam profile in angle and in energy is shown for the newly designed HRM with double Si 111 reflections. It consists of five reflections in the arrangement $(+,-,+,+,+)$. The obtained maximum throughput is 0.299. The incident beam at BL09XU has a vertical divergence of 2.0 arcsec in FWHM. Assuming a Gaussian profile with an FWHM of 2.0 arcsec, the energy spectrum of the throughput for the newly designed HRM is obtained by the calculation, as shown in Fig. 3 (a, solid red line). Its energy resolution is 0.86 meV. The same energy resolution is obtained using the symmetric Ge 331 reflection and two successive Si 975 reflections with $b = 1/17.0$ and 17.0 as well. The energy spectrum is also shown as a dotted blue line in Fig. 3(a). A total flux increase of 24% is achieved with the same energy resolution using the new design [Fig. 3(a), solid red line vs dotted blue line]. As mentioned in the introduction, this increase is significant for the NRVS of biological samples.

The angular acceptance profiles for the two optics designs are shown in Fig. 3(b). A Gaussian beam profile is not included in the calculation of Fig. 3(b). The wider angular acceptance profile of the new optics affords more stable output intensity to the beam fluctuation. If we adopt $b = 2 \times 10.8$ (or 21.6) instead of $b = 18.0$ for the last reflection to obtain the original beam size, the total flux will decrease by 11% with a 5% higher resolution. This flux decrease suggests that both the asymmetric reflection of Ge and the enlarged beam size contribute to the total flux increase.

As shown in Fig. 1(b), both the first and second Si 975 crystals are placed on the same base plate, which is attached to a high-precision goniometer (KOUZU KTG-15). Using this tangent bar goniometer, both crystals are rotated by the same amount to adjust the maximum intensity. The second Si 975 crystal is mounted on the stage with a tilting mechanism and a weak-link hinge. X-rays reflected from the Ge crystal

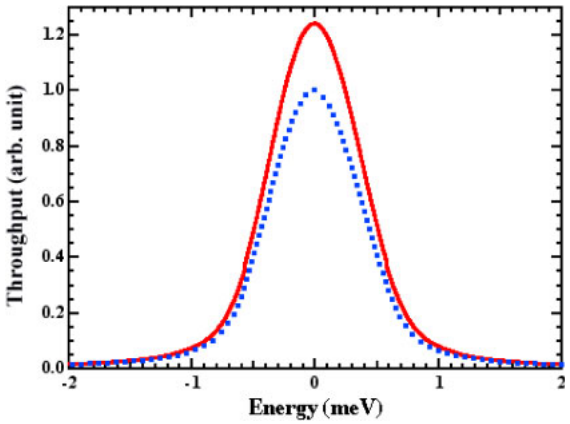

(a)

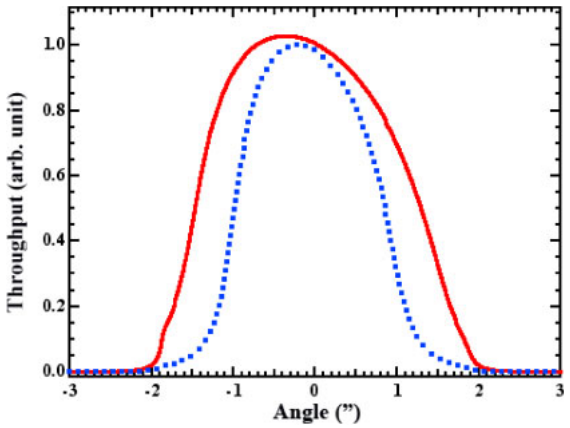

(b)

Fig. 3. (Color online) (a) Calculated energy spectra of the throughput for the newly designed HRM (solid line) and symmetric Ge 331 reflection + Si 975 reflections with $b = 1/17.0$ and 17.0 (dotted line). A Gaussian profile with an FWHM of 2.0 arcsec is assumed for the incident beam. (b) Calculated angular acceptance profiles for the newly designed HRM (solid line) and symmetric Ge 331 reflection + Si 975 reflections with $b = 1/17.0$ and 17.0 (dotted line). The Gaussian profile is not included in (b). Double Si 111 reflections prior to HRM are included in all calculations.

pass through a hole in the stage, as shown in Fig. 1(a). The angle between the two Si 975 crystals, which is essential for energy stability, is controlled by the piezoelectric linear stage (Physik Instrumente P-753.2CD) with a 25 μm stroke. Rotation is achieved using the tangent bar mechanism with setting the weak-link as the fulcrum line. The mechanical resolution of this stage is 1 nm and the repeatability, which is more important for long-term stability, is ±2 nm. This value corresponds to a resolution of ±0.025 meV, which is significantly better than the designed resolution of 0.86 meV. No corrections by the encoder or the temperature of the crystals are employed.

3. Experiments and results

Experiments were conducted at BL09XU, SPring-8.[14,15] X-rays from the in-vacuum undulator were filtered by a liquid-nitrogen-cooled high-heat load monochromator composed of double Si 111 reflections.[16,17] The undulator gap was 19.77 mm and the Bragg angle of Si 111 was set to 7.89° to match the resonant energy of Fe-57. The HRM was arranged in experimental hutch 1 for further monochromatization. The energy from the HRM was scanned by changing

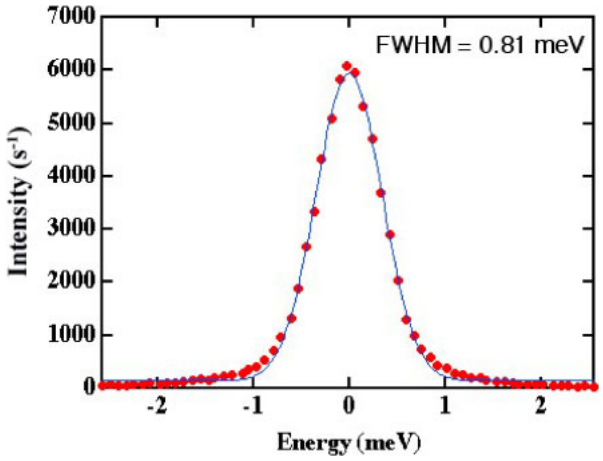

Fig. 4. (Color online) Measured energy resolution of the newly designed HRM. (Dots: experimental data, line: fitted Gaussian curve.) FWHM of 0.81 meV was obtained from the Gaussian fit.

the angle between the two Si 975 crystals while keeping the output intensity at its maximum by changing the angle of the base plate of the two Si 975 crystals.

The energy resolution of the HRM was measured using the transmission geometry of an Fe-57 foil placed after the HRM. The X-rays scattered by a Cu foil, which was isolated from the Fe-57 foil, were counted by means of an avalanche photodiode (APD) detector, although this scattering geometry is not essential for measuring the resolution. Four APDs with 1-mm separation were used to count the delayed signals. Each APD had $3 \times 5\,\mathrm{mm}^2$ area and a 150-μm-thick deletion layer.[18] The Fe-57 foil and APD detectors were arranged in experimental hutch 2. The Ge 331 crystal was fixed during the energy scan. The energy scale of the HRM output was calibrated by the NRVS of $(NEt_4)(^{57}FeCl_4)$ cooled in a cryostat.[19,20]

The measured resolution function of the HRM is shown in Fig. 4. The resolution obtained by Gaussian fitting was 0.81 meV (FWHM), which almost agrees with the calculated resolution of 0.86 meV. The flux measured by the photodiode at the sample position was 1.9×10^9 photons/s. The measured throughput of the HRM was 7.1×10^{-5}. Although this value is 59% of the calculated value of 1.2×10^{-4}, it is comparable with the previously reported values of 47% and 65% for the ratio of the experimental result to the calculated result in HRMs for Fe-57.[11,12] Therefore, the newly developed HRM has performed well and the higher throughput of the new design has been experimentally verified. The discrepancy between the experiment and calculation occurred in the asymmetric Si 975 reflections in our case. The following problems can be considered as possible reasons: fabrication errors in the asymmetric factors in Si 975, surface roughness and distortion, crystal imperfection, and difficulty in calculating the absolute reflectivity of higher order reflections using the dynamical theory.

Ideally, the resonant peak position remains constant in each scan. In practice, however, the peak position shifts or fluctuates due to temperature drift and/or mechanical drift of the crystal angles. The drift in the peak position over one day is shown in Fig. 5. The resonant peak position in each scan is plotted as a function of time. Each measurement scan lasted 1 h. Figure 5 clearly shows a gradual change in the position

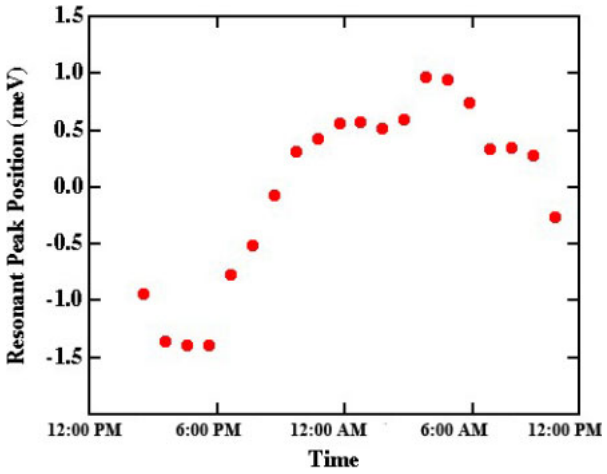

Fig. 5. (Color online) Resonant peak position in each scan over a period of one day.

of the peak resonant energy. The position shifts in one direction for a few hours, then the drift stops and then the position shifts in the opposition direction for a few hours. This suggests that the drift in resonant energy position is caused by drifts in temperature over one day, even though the air temperature in experimental hutch 1 is controlled by an air conditioner to within 0.1 °C. The data in Fig. 5 suggest that linear energy shifts between scans are reasonable as a first approximation. As mentioned in the introduction, the zero point of the phonon energy is calibrated from the resonant peak position for each NRVS scan. Moreover, the energy scale for each scan can also be calibrated by assuming linear energy shifts between scans. In other words, the stability of the new HRM is sufficient to maintain the intrinsic resolution. Another advantage of this higher stability is the ability to set as small a measuring energy range as necessary. Therefore, data loss at the edges of the energy range can be reduced.

4. Summary

A new high-resolution monochromator with higher flux for 14.4-keV X-rays has been designed and developed for the Fe NRVS of biological samples. Calculation using the dynamical theory of X-ray diffraction shows a 24% increase in flux while maintaining the resolution. A 20% increase of the exit beam size is acceptable to our biological applications. It must be mentioned that this flux increase is achieved by simply cutting the crystals in different directions. This HRM can also be used for any other samples besides biological samples. The measured resolution of 0.81 meV almost agrees with the calculated resolution of 0.86 meV. The higher throughput of the new design has been experimentally verified. The resulting stability is sufficient to preserve its intrinsic resolution and avoid degrading the spectra.

Acknowledgements

We thank Professor Kikuta for his encouragement and useful discussion. The experiments were performed at BL09XU of SPring-8 with the approval of the Japan Synchrotron Radiation Research Institute (JASRI) (Proposal Nos. 2011A2061, 2013B1928, and 2014A1887). This work was supported by KAKENHI (16H04172), a grant NIH (GM-65440), and CREST, JST.

1) M. Seto, Y. Yoda, S. Kikuta, X. W. Zhang, and M. Ando, Phys. Rev. Lett. **74**, 3828 (1995).
2) W. Sturhahn, T. S. Toellner, E. E. Alp, X. W. Zhang, M. Ando, Y. Yoda, S. Kikuta, M. Seto, C. W. Kimball, and B. Dabrowski, Phys. Rev. Lett. **74**, 3832 (1995).
3) Y. Xiao, K. Fisher, M. C. Smith, W. D. Newton, A. Case, S. J. George, H. Wang, W. Sturhahn, E. E. Alp, J. Zhao, Y. Yoda, and S. P. Cramer, J. Am. Chem. Soc. **128**, 7608 (2006).
4) S. D. Wong, M. Srnec, M. L. Matthews, L. V. Liu, Y. Kwak, K. Park, C. B. Bell, E. E. Alp, J. Zhao, Y. Yoda, S. Kitao, M. Seto, C. Krebs, J. M. Bollinger, and E. I. Solomon, Nature **499**, 320 (2013).
5) J. T. Sage, S. M. Durbin, W. Sturhahn, D. C. Wharton, P. M. Champion, P. Hession, J. Sutter, and E. E. Alp, Phys. Rev. Lett. **86**, 4966 (2001).
6) B. Moeser, A. Janoschka, J. A. Wolny, H. Paulsen, I. Filippov, R. E. Berry, H. Zhang, A. I. Chumakov, F. A. Walker, and V. Schünemann, J. Am. Chem. Soc. **134**, 4216 (2012).
7) M. G. I. Galinato, J. G. Kleingardner, S. E. J. Bowman, E. E. Alp, J. Zhao, K. L. Bren, and N. Lehnert, Proc. Natl. Acad. Sci. U.S.A. **109**, 8896 (2012).
8) Z. J. Tonzetich, H. Wang, D. Mitra, C. E. Tinberg, L. H. Do, F. E. Jenney, Jr., M. W. Adams, S. P. Cramer, and S. J. Lippard, J. Am. Chem. Soc. **132**, 6914 (2010).
9) S. Kamali, H. Wang, D. Mitra, H. Ogata, W. Lubitz, B. C. Manor, T. B. Rauchfuss, D. Byrne, V. Bonnefoy, F. E. Jenney, Jr., M. W. W. Adams, Y. Yoda, E. E. Alp, J. Zhao, and S. P. Cramer, Angew. Chem., Int. Ed. **52**, 724 (2013).
10) T. Ishikawa, Y. Yoda, K. Izumi, C. K. Suzuki, X. W. Zhang, M. Ando, and S. Kikuta, Rev. Sci. Instrum. **63**, 1015 (1992).
11) A. I. Chumakov, J. Metge, A. Q. R. Baron, H. Grünsteudel, H. F. Grünsteudel, R. Rüffer, and T. Ishikawa, Nucl. Instrum. Methods Phys. Res., Sect. A **383**, 642 (1996).
12) M. Yabashi, K. Tamasaku, S. Kikuta, and T. Ishikawa, Rev. Sci. Instrum. **72**, 4080 (2001).
13) T. S. Toellner, A. Alatas, A. Said, D. Shu, W. Sturhahn, and J. Zhao, J. Synchrotron Radiat. **13**, 211 (2006).
14) Y. Yoda, M. Yabashi, K. Izumi, X. W. Zhang, S. Kishimoto, S. Kitao, M. Seto, T. Mitsui, T. Harami, Y. Imai, and S. Kikuta, Nucl. Instrum. Methods Phys. Res., Sect. A **467–468**, 715 (2001).
15) Y. Yoda, Y. Imai, H. Kobayashi, S. Goto, K. Takeshita, and M. Seto, Hyperfine Interactions **206**, 83 (2012).
16) S. Yamamoto, X. W. Zhang, H. Kitamura, T. Shioya, H. Hara, T. Mochizuki, H. Sugiyama, Y. Yoda, S. Kikuta, and M. Ando, J. Appl. Phys. **74**, 500 (1993).
17) T. Mochizuki, Y. Kohmura, A. Awaji, Y. Suzuki, A. Q. R. Baron, K. Tamasaku, M. Yabashi, H. Yamazaki, and T. Ishikawa, Nucl. Instrum. Methods Phys. Res., Sect. A **467–468**, 647 (2001).
18) S. Kishimoto, Y. Yoda, M. Seto, S. Kitao, Y. Kobayashi, R. Haruki, and T. Harami, Nucl. Instrum. Methods Phys. Res., Sect. A **513**, 193 (2003).
19) M. C. Smith, Y. Xiao, H. Wang, S. J. George, D. Coucovanis, M. Koutmos, W. Sturhahn, E. E. Alp, J. Zhao, and S. P. Cramer, Inorg. Chem. **44**, 5562 (2005).
20) H. Wang, Y. Yoda, W. Dong, and S. D. Huang, J. Synchrotron Radiat. **20**, 683 (2013).